JEM Journal of Experimental Medicine

BRIEF DEFINITIVE REPORT

Requirements for cDC2 positioning in blood-exposed regions of the neonatal and adult spleen

Dan Liu[1,2], Jiaxi Wu[1,2], Jinping An[1,2], and Jason G. Cyster[1,2]

The marginal zone (MZ) of the spleen contains multiple cell types that are involved in mounting rapid immune responses against blood-borne pathogens, including conventional dendritic cells (cDCs) and MZ B cells. MZ B cells develop later than other B cell types and are sparse in neonatal mice. Here, we show that cDC2s are abundant in the MZ of neonatal compared with adult mice. We find that conditions associated with reduced MZ B cell numbers in adult mice cause increased cDC2 occupancy of the MZ. Treatment with the S1PR1-modulating drug, FTY720, causes cDC2 movement into the MZ through the indirect mechanism of displacing MZ B cells into follicles. Splenic cDC2s express high amounts of α4β1 and αLβ2 integrins and depend on these integrins and the adaptor Talin for their retention in blood-exposed regions of the spleen. Splenic CD4 T cell activation by particulate antigens is increased in mice with higher cDC2 density in the MZ, including in neonatal mice. Our work establishes requirements for homeostatic cDC2 positioning in the spleen and provides evidence that localization in blood-exposed regions around the white pulp augments cDC2 capture of particulate antigens. We suggest that MZ positioning of cDC2s partially compensates for the lack of MZ B cells during the neonatal period.

Introduction

Conventional dendritic cells (cDCs) are divided into two types: cDC1s, which are effective in antigen cross-presentation and activation of CD8 T cells, and cDC2s, which are efficient activators of CD4 T cells and contribute to T follicular helper cell responses, among others (Durai and Murphy, 2016). For cDCs to function as antigen-presenting cells, they must capture antigen efficiently, and this requires them to be located in places where antigen enters the body or is concentrated by fluid flow.

The spleen, the largest secondary lymphoid organ, is an important site for initiating immune responses against systemic pathogens. The spleen has an open blood circulation, with blood being released at the marginal sinus that surrounds the white pulp cords, as well as at terminal arterioles in the red pulp (Mebius and Kraal, 2005). Blood leaves the marginal sinus via fenestrations in its outer surface, and it travels through the marginal zone (MZ) before entering the red pulp to return to circulation. The MZ of adult mice contains an abundance of MZ B cells as well as MZ macrophages (MZMs), marginal metallophilic macrophages (MMMs), stromal cells, and cDCs (Mebius and Kraal, 2005).

At baseline, splenic cDC2s are present in greatest numbers in MZ bridging channels, regions of the white pulp cords where the T zone directly connects with the red pulp and where the MZ is absent (Dudziak et al., 2007; Eisenbarth, 2019; Yi and Cyster, 2013). A variable small fraction of cDC2s are also present in the MZ, red pulp, and white pulp. cDC1s are found in the red pulp, MZ, and T zone and are rare in the bridging channels. Following activation by a variety of stimuli such as LPS, polyinosinic-polycytidylic acid, or apoptotic cells, cDCs move into the T zone in a CCR7-dependent manner (Eisenbarth, 2019; Lu et al., 2017). Recent work has shown that cDC2 positioning in MZ bridging channels depends on EBV-induced G-protein–coupled receptor 2 (EBI2, aka GPR183) and two oxysterol ligands, 7α,25- and 7α,27-hydroxycholesterol (Gatto et al., 2013; Lu et al., 2017; Yi and Cyster, 2013). However, whether adhesion molecules are involved in bridging channel localization and what factors control positioning in the nearby MZ have not been clear.

Splenic MZ B cells are a specialized population of "rapid responder" B cells (Martin and Kearney, 2002). They are enriched for cells that recognize antigens present in bacterial membranes, and they can rapidly give rise to plasma cells upon antigen recognition. MZ B cells are also involved in delivering opsonized antigens from the blood-exposed MZ into follicles for long-term display to recirculating follicular B cells (Cinamon et al., 2008). The development of MZ B cells is delayed compared with follicular B cells and, as such, the MZ becomes occupied by B cells

[1]Howard Hughes Medical Institute, San Francisco, CA; [2]Department of Microbiology and Immunology, University of California, San Francisco, San Francisco, CA.

Correspondence to Jason G. Cyster: jason.cyster@ucsf.edu.

more slowly than the follicular compartment (Martin and Kearney, 2002). The slow development of MZ B cells is thought to contribute to the greater susceptibility of neonatal mice and humans to some types of blood-borne pathogens. Whether there are interim mechanisms acting in neonates to provide some amount of compensatory protection until MZ B cells develop is not known.

Here, we find that neonatal mice have a greater fraction of their cDC2s situated in the MZ than in adult mice. Examination of adult mice with reduced numbers of MZ B cells (*Cd19*$^{-/-}$ or MD4/ML5 mice) reveals increased occupancy of the MZ by cDC2s. Moreover, the ability of the S1PR1-modulating drug, FTY720, to promote cDC2 occupancy of the MZ is found to reflect its ability to relocate MZ B cells into follicles. We find that cDC2 retention and homeostasis in bridging channels and the MZ are dependent on integrins as well as the integrin adaptor Talin. In mice in which cDC2s are more abundant in the MZ, including neonatal mice, cDC2s capture particulate antigens more efficiently, and stronger helper T cell responses are supported.

Results and discussion

Increased MZ cDC2s in neonatal mice

The MZ B cell compartment is known to be underdeveloped in neonatal mice (Martin and Kearney, 2002), and we found that MZ B cells were approximately twofold less frequent in spleens of 3-wk-old mice compared with adults (Fig. 1 A). As expected, the neonatal mice also had fewer mature (CD23^{hi}) B cells (Fig. 1 A; Loder et al., 1999). However, the frequency of cDCs in the neonatal spleen was comparable to that in adults, and the fraction that expressed markers of cDC2 (DCIR2) and cDC1 (CD8) were equivalent (Fig. 1, B and C). An analysis of the tissue distribution of cDC2s by staining for DCIR2 (Dudziak et al., 2007) revealed that these cells were present in bridging channels in neonatal and adult mice, but in neonatal mice there were also many cDC2s located in the MZ (Fig. 1 D). We used DCIR2 rather than the more widely used marker CD4 to identify cDC2s in most cases, since this simplified detection of the DCs in tissue sections; costaining showed that the majority of DCIR2^{+} cDCs were CD4^{+} (Fig. S1 A). We have not distinguished the rarer CD4^{-} DCIR2^{+} cells from the CD4^{+} DCIR2^{+} cDC2s in this study.

In vivo pulse labeling with a PE-conjugated antibody can be used to quantitate the fraction of spleen cells that are in blood-exposed locations such as the MZ and outermost regions of the bridging channels (Calabro et al., 2016; Cinamon et al., 2008; Lu et al., 2017). In vivo antibody labeling with anti-CD45-PE showed that a similar proportion of MZ B cells became labeled in neonatal and adult mice (Fig. 1 E), indicating that the blood-exposed MZ B cells are reduced by an amount proportional to the overall reduction in MZ B cells. By contrast, a higher fraction of cDC2s were PE labeled in neonatal compared with adult mice (Fig. 1 F), in accord with a higher fraction of the cDC2s being situated in the MZ. Although not a focus of our study, a higher fraction of CD8^{+} cDC1s were also blood exposed in neonatal mice (Fig. S1 B). Immunofluorescent staining of spleen sections from adult mice injected with anti-CD11c-PE showed labeling of DCIR2^{+} cDC2s in the outer bridging channel, as well as rare cells in the MZ (Fig. S1 C). Analysis of sections from neonatal and adult mice treated with anti-CD45-PE showed bright staining of MZ cells in both cases, most likely including macrophages and B cells. However, in neonatal mice, there was also considerable PE labeling of DCIR2^{+} cDC2s in the MZ (Fig. S1 D).

Increased MZ cDC2s in mice with reduced MZ occupancy by B cells

The findings in neonatal mice led us to speculate that there might be competition for MZ niche occupancy between MZ B cells and cDC2s. To explore this hypothesis, we irradiated WT mice and reconstituted their hematopoietic systems with *Cd19*$^{-/-}$ bone marrow (BM) cells. These CD19-deficient chimeras had few MZ B cells (Fig. 2 A) and normal frequencies of cDC2s, but in vivo antibody labeling showed that more of the cDC2s were blood exposed (Fig. 2 B). In contrast, cDC1s did not show an increase in PE labeling in these mice (Fig. S2 A). Staining of tissue sections showed that more of the cDC2s were located in the MZ than in control BM chimeras (Fig. 2 C), in accord with a prior report (You et al., 2009).

As another model to test whether a lack of B cells in the MZ was sufficient to cause cDC2 accumulation in this region, we examined Ig-transgenic (MD4) mice that also expressed the cognate antigen hen egg lysozyme (HEL; ML5 transgenic). In these mice, all the B cells are anergic owing to chronic exposure to HEL autoantigen, and MZ B cells are almost absent (Fig. 2 D; Mason et al., 1992). Although the cDC2 frequency in these mice was normal, in vivo antibody labeling showed an increased fraction of blood-exposed cDC2s (Fig. 2 E). Labeling of cDC1s was not significantly increased (Fig. S2 B). Analysis of spleen sections from MD4/ML5 mice showed increased cDC2 occupancy of the MZ (Fig. 2 F).

Treatment with the S1PR1 functional antagonist FTY720 causes rapid displacement of MZ B cells out of the MZ and their entrapment within follicles (Fig. 2 G; Cinamon et al., 2004). In agreement with an earlier study (Czeloth et al., 2007), FTY720 treatment led to cDC2 accumulation in the MZ (Fig. 2 H). In vivo antibody pulse labeling showed that an increased fraction of the cDC2s were blood exposed (Fig. 2 H and Fig. S1 E). The previous report had suggested that FTY720 was acting directly via S1PR1 on cDC2s to cause redistribution into the MZ (Czeloth et al., 2007). However, splenic cDC2s do not detectably express S1PR1 mRNA or protein (Fig. 2, I and J), consistent with findings in S1PR1-eGFP reporter mice (Cahalan et al., 2011). To formally test whether S1PR1 was required in cDC2s, we reconstituted WT mice with *S1pr1*$^{f/f}$ *CD11c-Cre* BM and then treated the animals with saline or FTY720. Deletion of the *S1pr1* coding exon in cDCs was confirmed by PCR (Fig. S2 C). S1PR1 deletion did not modify baseline cDC2 localization, and FTY720 treatment continued to be effective in promoting cDC2 redistribution to the MZ (Fig. 2, K and L).

To further test if the action of FTY720 was through functional antagonism of MZ B cell S1PR1, we reconstituted WT mice with *S1pr1*$^{f/f}$ *Mb1-Cre* BM. S1PR1 deletion from MZ B cells was confirmed by qPCR and FACS (Fig. 2, I and J). In these mice, MZ B cells (IgM^{hi}IgD^{lo} cells) were mostly absent from the MZ owing

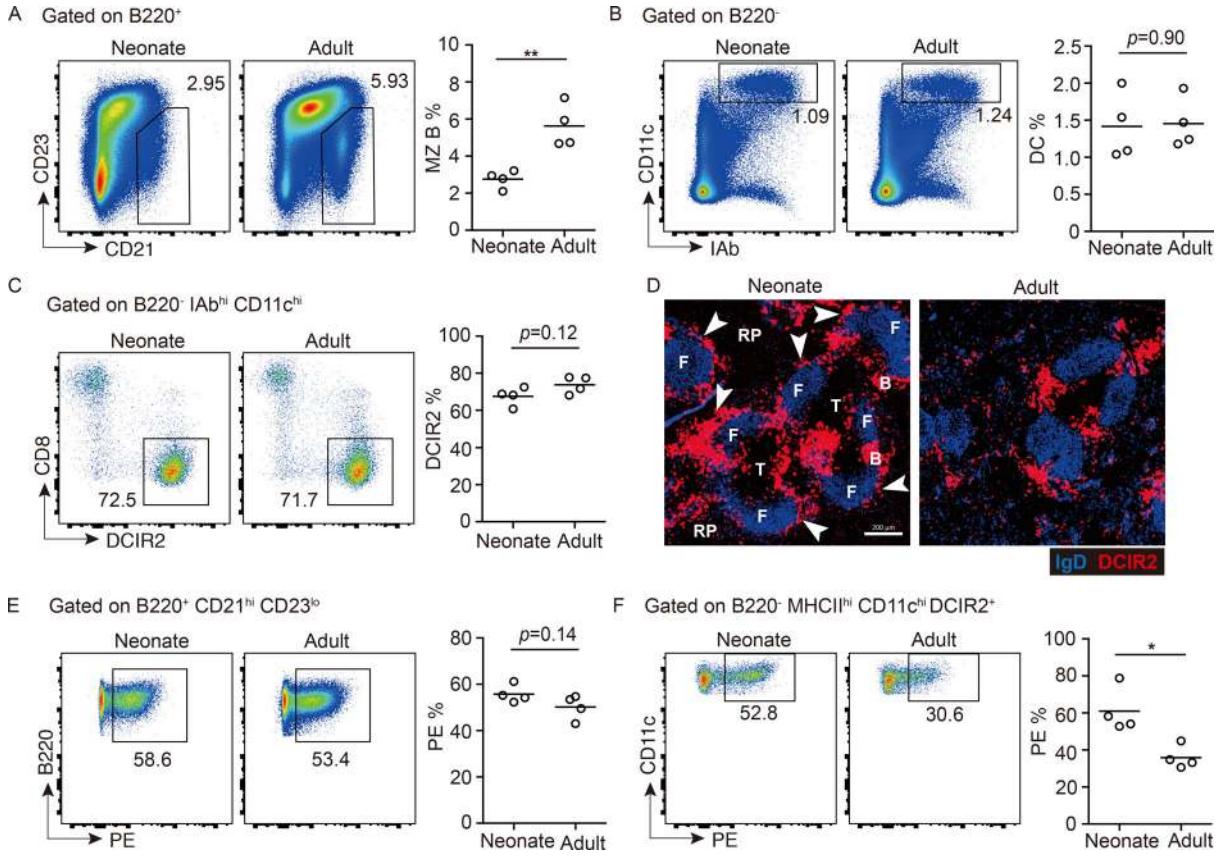

Figure 1. **Increased MZ cDC2s in neonatal mice. (A–C)** Representative FACS profiles and frequencies of CD21^{hi} CD23^{lo} MZ B cells in total B220^{+} B cells (A), CD11c^{hi} I-Ab^{hi} DCs in total B220^{-} lymphocytes (B), and DCIR2^{+} cDC2s in total DCs (C) in neonatal (3 wk old) and adult (8–12 wk old) mice. **(D)** Representative distribution patterns of DCIR2^{+} cDC2s (red) relative to IgD^{+} B cells (blue) in spleens of mice of indicated ages. Arrowheads in left panel point to DCIR2^{+} DCs in the MZ. F, follicle; RP, red pulp; T, T cell zone; B, bridging channel. Scale bar, 200 µm. **(E and F)** FACS profiles and frequencies of in vivo anti-CD45-PE–labeled MZ B cells (E) and cDC2s (F) in mice of indicated ages. Each symbol represents one mouse, and lines denote means. In each case, one of three independent experiments with similar results is shown, in which each group had at least three mice. Sections are representative of multiple cross sections from six mice of each type. *, P < 0.05; **, P < 0.01.

to trapping within follicles (Fig. 2 N and Fig. S2 D), as expected (Cinamon et al., 2004). Importantly, cDC2s (Fig. 2 M) but not cDC1s (Fig. S2 E) were more blood exposed, and DCIR2^{+} cDC2s were enriched within the MZ (Fig. 2 N). These data indicate that FTY720 acts via an indirect mechanism to promote cDC2 positioning in the MZ and are consistent with the redistribution occurring secondary to the displacement of MZ B cells from this region.

We also attempted to test the effect of increasing the B cell content of the MZ on cDC2 distribution. Mice deficient in CXCR5 have a higher frequency of MZ B cells in the spleen and many B cells located in the MZ (Fig. S2 F; Ansel et al., 2000). However, these mice also have very few B cells situated within follicles. Tissue section analysis revealed that the cDC2s in CXCR5 KO mice were excluded from the MZ and instead were most abundant in the primitive follicles (Fig. S2 G). In accord with their being enriched within the white pulp, cDC2s in CXCR5 KO mice were protected from in vivo PE antibody labeling (Fig. S2 H). We speculate that in the poorly occupied B cell follicles in these mice, EBI2 ligand availability is increased, and this distorts the EBI2 ligand distribution that normally promotes cDC2 positioning in the bridging channels, leading to their accumulation in the underoccupied follicles.

Given these findings, we instead took the approach of reconstituting the MZ of *Cd19*$^{-/-}$ mice with CXCR5-deficient B cells using a previously established adoptive transfer approach (Fig. S2 I; Arnon et al., 2013). Consistent with an earlier study (Cinamon et al., 2008), MZ B cells (IgM^{hi}IgD^{lo} cells) lacking CXCR5 were not able to migrate into follicles after FTY720 treatment (Fig. S2 J). Importantly, FTY720 treatment failed to promote increased blood exposure or MZ positioning of cDC2s in these mice (Fig. S2, K and L). These data provide further support for the conclusion that cDC2 access to the MZ is restrained by MZ B cells.

Depletion of macrophages does not increase cDC2 occupancy of the MZ

SIGN-R1^{+} and MARCO^{+} MZMs and CD169^{+} MMMs are major occupants of the splenic MZ. In contrast to the effects of MZ B cell deficiency, depletion of MZMs and MMMs using clodronate liposomes did not increase cDC2 occupancy of the MZ as measured by in vivo antibody labeling (Fig. 3 A) or staining of sections (Fig. 3 B). The treatment did not modify MZ B cell distribution between MZ and follicles, as assessed by in vivo antibody labeling (Fig. 3 C). In a second approach, we ablated

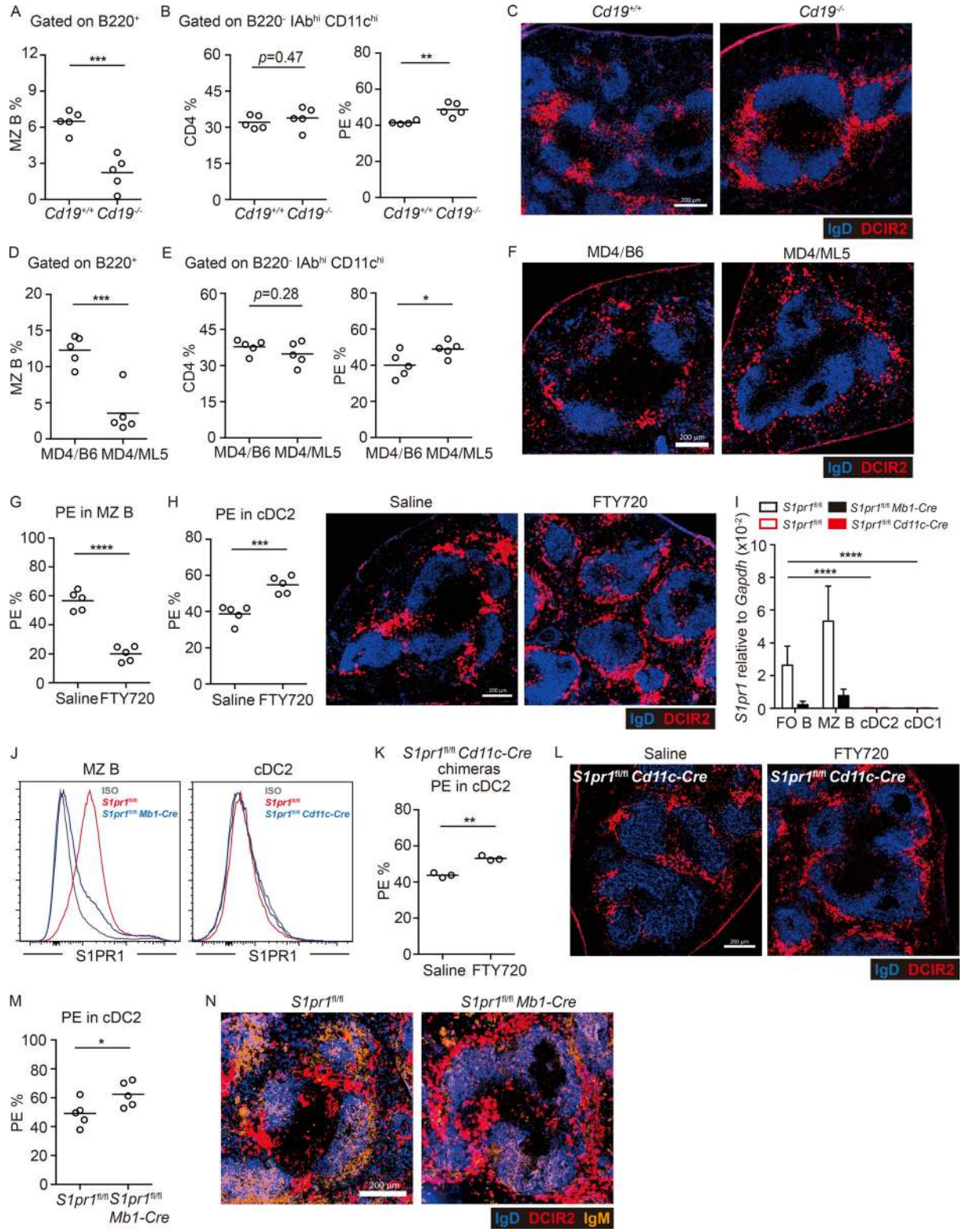

Figure 2. **Increased MZ cDC2 in mice with reduced MZ occupancy by B cells. (A–C)** Frequencies of CD21^{hi} CD23^{lo} MZ B cells in total B220^{+} B cells (A), and CD4^{+} cDC2s in DCs (B, left) and in vivo anti-CD45-PE–labeled cDC2s (B, right) and representative distribution patterns of DCIR2^{+} cDC2s (red) relative to B cells (blue) in spleens (C) of indicated genotyped BM chimeras. **(D–F)** Ig-transgenic MD4 BM cells were used to reconstitute irradiated C57BL/6J or ML5-transgenic mice. Frequencies of MZ B cells in total B220^{+} B cells (D) and CD4^{+} cDC2s in DCs (E, left) and in vivo anti-CD45-PE–labeled cDC2s (E, right) and representative distribution patterns of DCIR2^{+} cDC2s (red) relative to B cells (blue) in spleens (F) of indicated BM chimeras. Each symbol represents one mouse, and lines denote means. Data are pooled from two independent experiments. **(G and H)** Frequencies of in vivo anti-CD45-PE labeling of MZ B cells (G) and cDC2s (H, left) or representative distribution patterns of DCIR2^{+} cDC2s (red) relative to B cells (blue) in spleens (H, right) 4 h after FTY720 or saline treatment. Each symbol represents one mouse, and lines denote the means. One of three independent experiments with similar results is shown. **(I)** Quantitative PCR analysis of *S1pr1*

in sorted MZ B cells (B220$^+$ CD21^{hi} CD23^{lo}) and follicular (FO) B cells (B220$^+$ CD23^{hi} CD21^{int}) from control (hollow black) and *S1pr1*-B cell–deficient (solid black) BM chimeras or sorted cDC2s (CD11c^{hi} MHCII^{hi} DCIR2$^+$) and cDC1s (CD11c^{hi} MHCII^{hi} CD8$^+$) from control (hollow red) and *S1pr1*-DC–deficient (solid red) BM chimeras, calculated as relative amount of mRNA normalized to *Gapdh*, $2^{-\Delta Ct}$. Bars represent mean (± SD) of four experiments. **(J)** Representative histograms of S1PR1 in MZ B cells (left) and cDC2s (right) in BM chimeras of the indicated genotype. **(K and L)** Frequencies of in vivo anti-CD45-PE–labeled cDC2s (K) and representative distribution patterns of DCIR2$^+$ cDC2s (L, red) relative to B cells (blue) in spleens with 4-h FTY720 or saline treatment in *S1pr1*-DC–deficient BM chimeras. One of two independent experiments with similar results is shown, with at least three mice in each group. **(M and N)** Frequencies of in vivo anti-CD45-PE–labeled cDC2s (M) and representative distribution patterns of DCIR2$^+$ cDC2s (N, red) and MZ B cells (orange) relative to B cells (blue) in spleens in control and *S1pr1*-B cell–deficient BM chimeras. Each symbol represents one mouse, and lines denote means. Data are pooled from two independent experiments. Scale bar, 200 µm. Sections are representative of multiple spleen cross sections from at least three mice of each type. *, P < 0.05; **, P < 0.01; ***, P < 0.001; ****, P < 0.0001.

CD169$^+$ macrophages by diphtheria toxin treatment of CD169-DTR mice. This treatment ablates both MMMs and MZMs (Miyake et al., 2007). The loss of these macrophage populations was not sufficient to significantly modify the localization of cDC2s or MZ B cells (Fig. 3, D–F).

Integrins and integrin adaptor Talin are required for cDC2 lodgment in blood-exposed locations

Past work has shown that MZ B cell retention in the MZ depends on their higher expression of integrins α4β1 and αLβ2 than follicular B cells (Lu and Cyster, 2002). Flow cytometric analysis showed that cDC2s had high expression of α4β1 and αLβ2 integrins (Fig. 4 A). Talin is a critical adaptor protein for integrin function (Calderwood et al., 2013). Talin-deficient mice have a reduction in their cDC2 compartment size (Fig. 4 B; Wu et al., 2018). Contrasting with their reduced frequency in the spleen, cDC2s were markedly increased in blood (Fig. 4 C). In vivo antibody labeling showed that a reduced fraction of Talin-deficient splenic cDC2s were blood exposed (Fig. 4 D). In contrast, cDC1 antibody labeling was unchanged in Talin-deficient mice (Fig. S3 A). Tissue section analysis showed that DCIR2$^+$ cDC2s were reduced from the bridging channels and MZ (Fig. 4 E). When cDCs were injected directly into the blood, they were almost undetectable within 3 h (Fig. S3 B), indicating they have a very short survival time in circulation. Therefore, the elevated frequency of Talin-deficient cDC2s in blood is consistent with their continuous loss into blood, leading to a lower frequency of blood-exposed cDC2s resident within the spleen. After FTY720 treatment, Talin-deficient cDC2s were underrepresented in the MZ (Fig. 4 E).

The role of individual integrins was examined using gene-deficient mice. In mice lacking the Itgb1 chain selectively in CD11c$^+$ cells, there was a reduction in splenic cDC2 frequency (Fig. 4 F), more cells were detected in blood circulation (Fig. 4 G), and a reduced fraction of the splenic cDC2s were blood exposed, as determined by in vivo antibody labeling and section analysis (Fig. 4, H and I). There was also little ability to accumulate in the

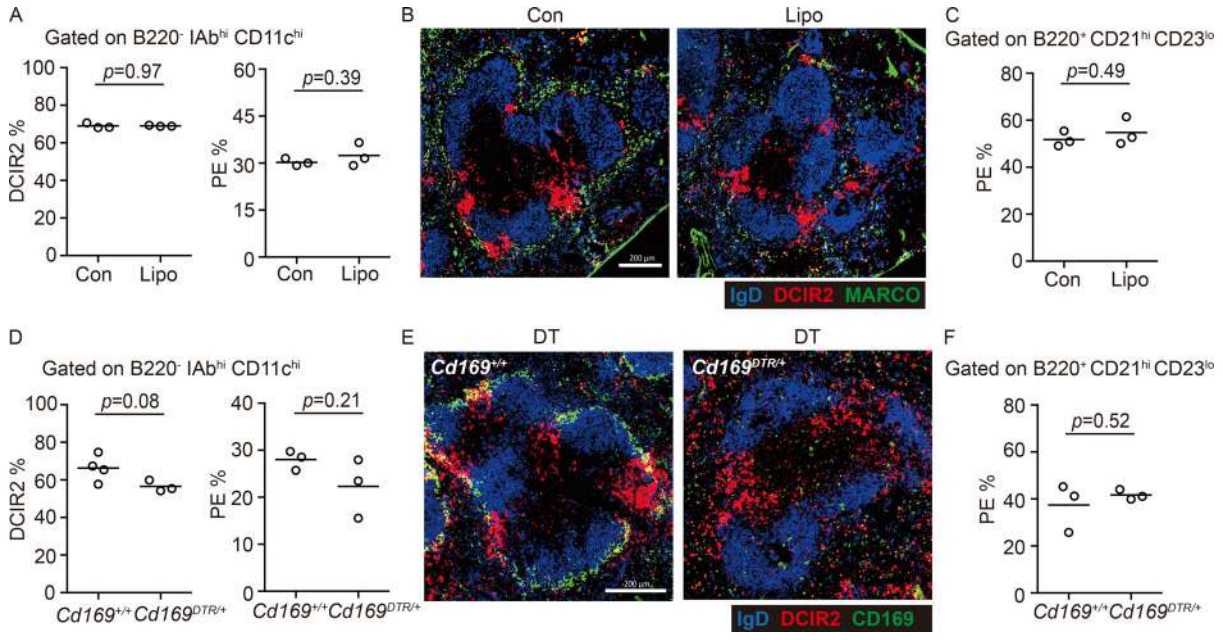

Figure 3. **Macrophages are dispensable for exclusion of splenic cDC2s from the MZ. (A and B)** Frequencies of DCIR2$^+$ cDC2s in DCs (A, left) or in vivo anti-CD45-PE labeling of cDC2s (A, right) and representative distribution patterns of MARCO$^+$ MZMs (green) and DCIR2$^+$ cDC2s (red) relative to IgD$^+$ B cells (blue) in spleens (B) 2–3 wk after clodronate liposome (Lipo) or control (Con) treatment. **(C)** In vivo anti-CD45-PE labeling of MZ B cells in mice in A. **(D and E)** Frequencies of DCIR2$^+$ cDC2s in total DCs (D, left) or in vivo anti-CD45-PE labeling of cDC2s (D, right) and representative distribution patterns of CD169$^+$ MMMs (green) or DCIR2$^+$ cDC2s (red) relative to IgD$^+$ B cells (blue) in spleens (E) 2–3 d after diphtheria toxin (DT) treatment in *CD169*$^{DTR/+}$ and control mice. **(F)** In vivo anti-CD45-PE labeling of MZ B cells in mice in D. Each symbol represents one mouse, and lines denote means. One of three independent experiments with similar results is shown. Sections are representative of of multiple spleen cross sections from six mice of each type. Scale bar, 200 µm.

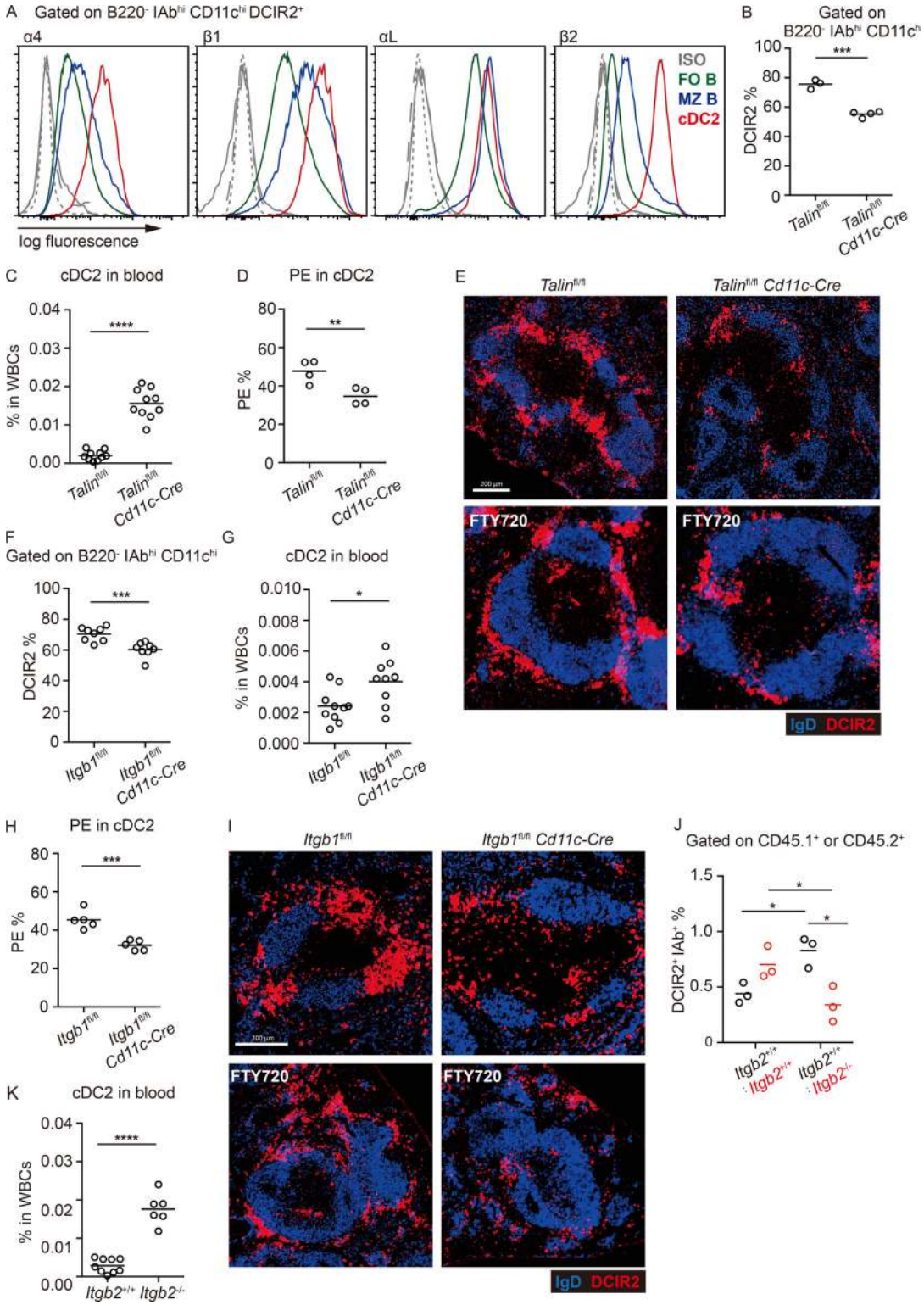

Figure 4. **Integrins and integrin adaptor talin are required in splenic cDC2s. (A)** Representative histogram plots of cell surface integrins on MZ B cells (blue line), follicular B cells (FO B; green line), and cDC2s (red line). Gray lines are staining controls for MZ (dash) and follicular (dot) B cells and cDC2s (solid). **(B and C)** Frequencies of DCIR2$^+$ cDC2s in spleen (B) and blood (C) in *Cd11c-Cre Talin*$^{fl/fl}$ and control mice. **(D)** Frequencies of in vivo anti-CD45-PE–labeled cDC2s in spleens of mice of the indicated genotypes. **(E)** Representative distribution patterns of DCIR2$^+$ cDC2s (red) relative to B cells (blue) in spleens of untreated (upper panel) and 15-h FTY720-treated (lower panel) mice of the indicated genotypes. Scale bar, 200 µm. **(F and G)** Frequencies of DCIR2$^+$ cDC2s in spleens (F) and blood (G) in *Cd11c-Cre Itgb1*$^{fl/fl}$ and control mice. **(H)** Frequencies of in vivo anti-CD45-PE–labeled cDC2s in spleens of mice of the indicated genotypes. **(I)** Representative distribution patterns of DCIR2$^+$ cDC2s (red) relative to B cells (blue) in spleens of untreated (upper panel) and 15-h FTY720-treated (lower panel) mice of the indicated genotypes. Scale bar, 200 µm. **(J)** Frequencies of DCIR2$^+$ IAb$^+$ cDC2s in spleens of *Itgb2*$^{+/+}$ (CD45.1$^+$):*Itgb2*$^{+/+}$ (CD45.2$^+$) and *Itgb2*$^{+/+}$ (CD45.1$^+$):*Itgb2*$^{-/-}$ (CD45.2$^+$) mixed BM chimeras. Two-way ANOVA was applied. **(K)** Frequencies of DCIR2$^+$ cDC2s in blood of 4-wk-old

Itgb2$^{-/-}$ and control mice. Each symbol represents one mouse, and lines denote means. Data for cDC2s in blood and F are pooled from two independent experiments. For other data, one of two independent experiments with similar results is shown. Sections are representative of multiple spleen cross sections from six mice of each type. *, P < 0.05; **, P < 0.01; ***, P < 0.001; ****, P < 0.0001.

MZ after FTY720 treatment (Fig. 4 I). To test the role of Itgb2 in splenic cDC2 positioning, it was necessary to generate mixed BM chimeras, since adult Itgb2 KO mice have splenomegaly. Flow cytometric analysis of cDC2s in the mixed BM chimeras showed that Itgb2 deficiency led to reduced cDC2 representation in the spleen (Fig. 4 J). Interestingly, these mice showed an increased frequency of WT cDC2s, perhaps indicating that the loss of Itgb2-deficient cDC2s increased the niche available for occupancy by WT cells (Fig. 4 J). In accord with a reduced ability to occupy the splenic niche, analysis of full Itgb2 KO mice at 4 wk of age, before they develop splenomegaly, showed a marked elevation of cDC2s in the blood (Fig. 4 K).

Finally, as an approach to further distinguish between development roles versus constitutive requirements, we treated mice for 15 h with a combination of anti-α4 and -αL integrin–blocking antibodies. This led to a reduction in splenic cDC2 in vivo antibody labeling, and few cDC2s could be detected in MZs (Fig. S3, C–E). Staining for SIGNR1 and CD169 showed that the integrin-blocking antibody treatment did not notably alter MZM or MMM distribution, and IgD^{+} follicular B cell organization was maintained (Fig. S3 E). When the integrin-blocking antibody treatment was combined with FTY720 treatment, cDC2s were less efficient at accumulating in the MZ (Fig. S3, F and G). These findings are in accord with the genetic experiments, but we recognize that the possibility of indirect effects of the integrin-blocking antibody treatment cannot be excluded. Overall, these findings provide evidence that integrin-mediated adhesion is important for cDC2 retention and maintenance in splenic bridging channels and MZ.

Localization in blood-exposed regions favors particulate antigen capture and presentation

Sheep RBC (SRBC) immunizations are frequently used to study the splenic response to blood-borne particulate antigen. Splenic CD4 T cell responses to foreign RBCs depend strongly on cDC2s, as defined by the defective responses in mice deficient in cDC2s due to loss of Notch2, Irf4, CD47, or Dock8 (Briseño et al., 2018; Calabro et al., 2016; Lewis et al., 2011; Li et al., 2016). After FTY720 treatment, cDC2s captured greater amounts of PKH26-labeled SRBCs than did cDC2s in saline-treated control mice (Fig. 5 A). After an encounter with SRBCs, cDC2s become activated owing to missing self-CD47 recognition (Yi et al., 2015). In accord with the greater exposure to SRBCs, cDC2s in FTY720-treated mice were more strongly activated, as assessed by CD86 up-regulation (Fig. 5 B). To test whether the greater antigen capture and activation led to a more robust CD4 T cell activation, mice harboring OTII T cells were treated with saline or FTY720 and immunized with OVA-coupled SRBCs. The OTII T cells underwent greater proliferation in 3 d, and more of the cells became CXCR5^{hi}PD1^{hi} in the FTY720-treated mice (Fig. 5, C and D). By contrast, immunization with a nonparticulate antigen, LPS plus OVA, led to an equivalent response in FTY720-treated and control mice (Fig. 5 E). In accord with cDC2s being able to drive comparable T cell responses in cases where antigen access is not spatially restricted, movement of LPS plus soluble OVA-activated cDC2s to the T zone occurred comparably in control and FTY720-treated mice (Fig. S3 J). Analysis of FTY720-treated mice at day 6 of the OVA-SRBC response showed that the higher frequency of CXCR5^{hi}PD1^{hi} T follicular helper cells was maintained (Fig. S3 H). However, this was not associated with an elevated germinal center response (Fig. S3 I), perhaps because the lymphopenia induced by FTY720 treatment constrains other aspects of the early B cell response.

A similar analysis of the OTII T cell response to OVA-SRBC in CXCR5-deficient mice, in which there is a paucity of cDC2s in the MZ or in bridging channels, showed less efficient SRBC capture, cDC2 activation, and T cell proliferation than in control mice (Fig. S2, M–O). The defective T cell response in CXCR5-deficient mice was not due to an overall cDC2 defect, as induction of T cell proliferation in response to LPS and soluble OVA immunization was intact (Fig. S2 P).

Finally, analysis of neonatal mice showed that cDC2s more efficiently captured SRBCs (Fig. 5 F), more of the cells up-regulated CD86 (Fig. 5 G), and transferred OTII cells were more efficient at proliferating and becoming CXCR5^{hi}PD1^{hi} cells than in adult mice (Fig. 5, H and I). Immunization with a nonparticulate antigen led to similar amounts of proliferation and similar induction of CXCR5^{hi}PD1^{hi} on OTII T cells in neonatal and adult recipient mice (Fig. 5, J and K). Although we recognize that there are many differences between the spleens of neonatal and adult mice, these correlative observations suggest that MZ positioning of cDC2s augments their ability to acquire particulate antigens for presentation to CD4 T cells.

Concluding remarks

This study defines requirements for cDC2 positioning in blood-exposed regions of the spleen, a behavior that augments their ability to capture blood-borne particulate antigen for presentation to CD4 T cells. By showing that at least three conditions of reduced B cell occupancy of the MZ lead to increased cDC2 presence in this region, we provide evidence for a competition between MZ B cells and cDC2 for MZ occupancy. We find that a key requirement for positioning in blood-exposed locations around the white pulp, integrin-mediated adhesion, is shared between MZ B cells and cDC2s. The MZ contains ICAM1- and VCAM1-expressing stromal cells that support integrin-mediated adhesion of MZ B cells (Lu and Cyster, 2002) and likely also support attachment of cDC2s. The basis for the competition between MZ B cells and cDC2s for MZ occupancy might involve direct competition for "space" on the stromal cells. MZ B cells are continually motile while in the MZ, and they rapidly exchange between the MZ and follicle (Arnon et al., 2013). Because they are not rigidly occupying space on the stroma but are moving over it, a physical competition for space, while possible, seems

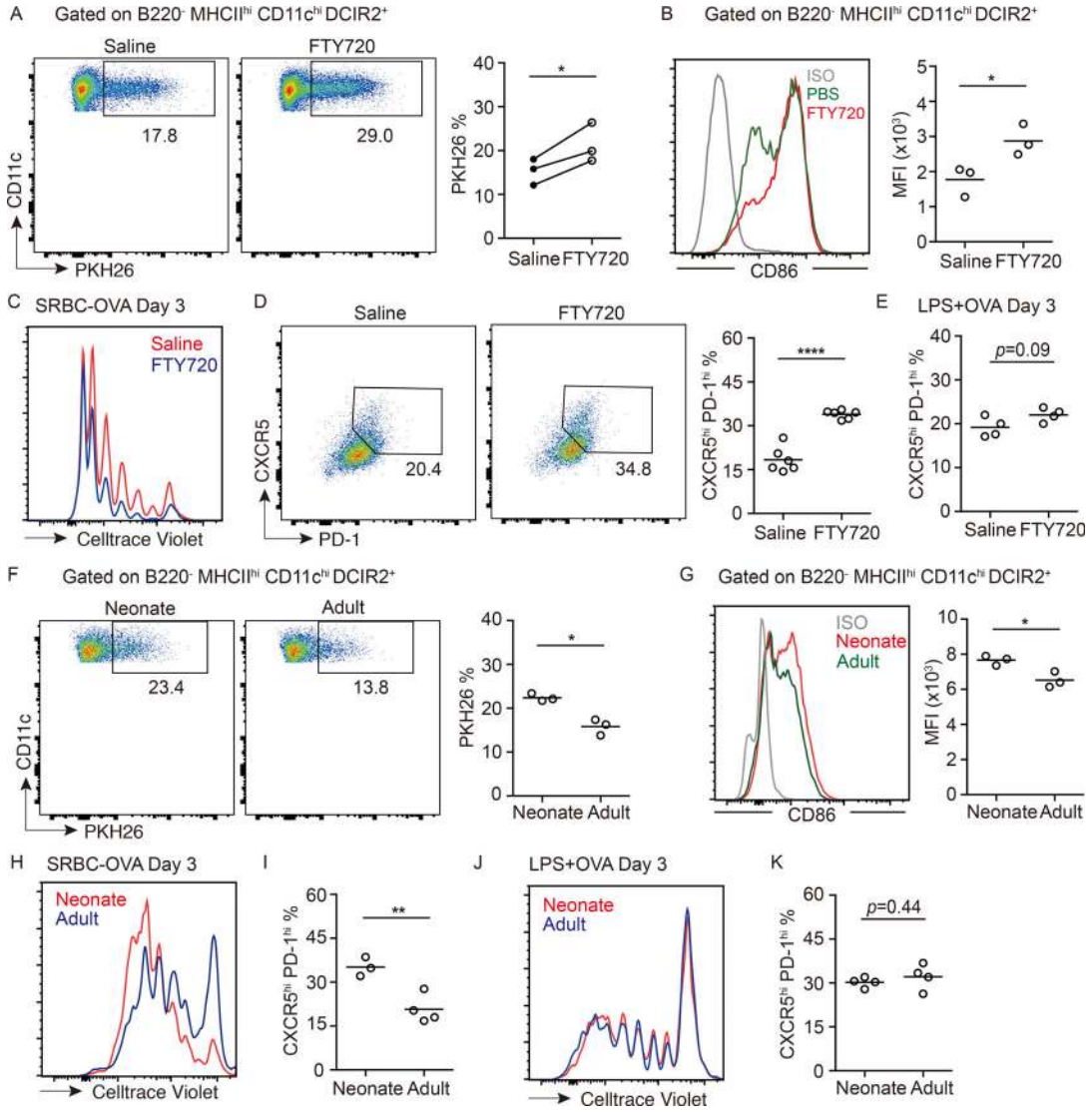

Figure 5. **MZ localization of cDC2s augments particulate antigen capture and CD4 T cell responses. (A)** Representative FACS plot and frequencies of PKH26-dye acquisition in DCIR2⁺ cDC2s from 4-h saline- or FTY720-treated mice, 3 h after PKH26-labeled SRBC immunization. Each symbol represents one independent experiment, and each line in the graph represents a paired experiment, with at least three mice in each group per experiment. **(B)** Geometric mean fluorescence intensity (MFI) and representative histogram of surface CD86 expression on cDC2s from mice treated as in A. **(C–E)** Representative FACS plot of proliferation (C) and CXCR5^{hi} PD-1^{hi} T cell gating (D, left) and frequencies of CXCR5^{hi} PD-1^{hi} T cells (D, right; and E) among transferred OT-II T cells in 4-h FTY720- or saline-pretreated mice, 3 d after SRBCs-OVA (C and D) or soluble OVA plus LPS (E) immunization. **(F)** Representative FACS plot and frequencies of PKH26⁺ cells in DCIR2⁺ cDC2s of neonatal or adult mice 3 h after immunization with PKH26-labeled SRBCs. **(G)** MFI and representative histogram of surface CD86 expression on cDC2s from mice treated as in F. **(H–K)** Representative FACS plot of proliferation and frequencies of CXCR5^{hi} PD-1^{hi} T cells in transferred OT-II T cells in indicated mice at day 3 after SRBC-OVA (H and I) or soluble OVA plus LPS (J and K) immunization. Each symbol represents one mouse, and lines denote means. One of two independent experiments with similar results is shown. *, P < 0.05; **, P < 0.01; ****, P < 0.0001.

an insufficient model to explain our observations. Another possibility is that MZ B cells deplete or suppress some property of another MZ cell type, perhaps a stromal cell, that promotes cDC2 recruitment or retention. A further possibility is that MZ B cells establish, either directly or indirectly, local production of "repellent" molecules that limit cDC2 access to this compartment.

We demonstrate that the role of S1PR1 in restraining cDC2 access to the MZ (Czeloth et al., 2007) is not cell intrinsic but rather occurs indirectly, owing to a role of S1P-S1PR1 in promoting MZ B cell positioning in the MZ. The rapid accumulation of cDCs in the MZ following FTY720-mediated displacement of MZ B cells suggests that cDCs may normally be accessing this region. We speculate that cDC2s undergo a shuttling behavior between the MZ and bridging channels akin to the shuttling of MZ B cells between the MZ and follicle (Arnon et al., 2013; Cinamon et al., 2008). The cDC2 compartment has a strong dependence on Notch2 and the ligand Delta-like 1 (Caton et al., 2007; Fasnacht et al., 2014; Lewis et al., 2011; Satpathy et al., 2013). Although the exact location of the necessary Delta-like 1–expressing cells is not fully defined (Fasnacht et al., 2014), the homeostatic migration behavior of cDC2s may be important

for their access to this stromal signal. Integrin- and Talin-dependent adhesion would be important for the cDC2s to resist the shear forces that are thought to occur in the MZ that can "flush" cells into the red pulp and blood circulation (Arnon et al., 2013). We suggest that shear forces are also operating on some cDC2s within the bridging channels given that intravascular antibody labels cDC2s in the outer (red pulp facing) segment of the bridging channel (Fig. S1; Calabro et al., 2016). It is also possible that integrins contribute to retention of cDC2s within the red pulp. The marked reduction in cDC2 numbers in Talin- and integrin-deficient mice, and the appearance of cDC2s in the blood of these mice, might reflect shear-mediated displacement of cells from the outer regions of the bridging channels as well as from the MZ. Recent work has shown that shear forces cause T cells and MZ B cells to migrate against the flow when adherent on ICAM1 and to migrate in the direction of flow when adherent on VCAM1 (Dominguez et al., 2015; Tedford et al., 2017). It seems reasonable to speculate that cDC2s will show similar migration behaviors under shear-exposed conditions, and this may be another factor contributing to their movement. ICAM1 and VCAM1 are present in bridging channels, although they are more abundant in the MZ (Lu and Cyster, 2002; Tedford et al., 2017). A previous study suggested cooperation between ICAM1 and MAdCAM1 in MZ positioning of cDC2 in FTY720-treated mice (Czeloth et al., 2007). Although the ICAM1 finding is consistent with our observations, we did not observe any effect of cDC2 deficiency in the MAdCAM1-binding integrin, α4β7, in our studies (unpublished data). The role of MAdCAM1 may therefore be indirect, perhaps through effects on the vasculature (Czeloth et al., 2007). After ruling out an intrinsic role for S1PR1 in cDC2 migration to the MZ, we tested four other Gαi-coupled receptors using inhibitors (for CXCR4 and EBI2) or KO mice (Cnr2 and Gpr43) and found that none of them were required for cDC2 movement to the MZ after FTY720 treatment (unpubished data). It remains possible that there is redundancy between some of these receptors or that another undefined chemoattractant receptor is involved.

We speculate that in adult mice the dominant occupancy of the MZ by MZ B cells, specialized rapid-responding innate-like lymphocytes, rather than by cDC2s, provides for a more optimized adaptive immune response against various systemic pathogens that are not modeled in our current work (Balázs et al., 2002; Martin and Kearney, 2002). The basis for the delayed maturation of the MZ B cell compartment in rodents and humans is not well defined, but it is thought to contribute to reduced antibody responses against T cell–independent antigens in neonates (Martin and Kearney, 2002). However, neonates are able to mount effective T-dependent immune responses against a range of antigens, including particulate antigens (Forsthuber et al., 1996; Ridge et al., 1998; Sarzotti et al., 1996). Recognizing that our observations are correlative, we suggest that the greater occupancy of the neonatal MZ by cDC2s augments the capacity to respond to blood-borne particulate antigens and reduces the vulnerability to infection during the period of neonatal development when passive immunity wanes and MZ B cell development is not yet complete.

Materials and methods

Mice

B6 (NCI 556) and B6-Ly5.2 (CD45.1; NCI 564) mice were purchased from National Cancer Institute at Charles River at age 6–8 wk. *Talin*$^{fl/fl}$ (Petrich et al., 2007) and *Cd11c-cre* (MGI: 3763248) mice were provided by K. Ley (La Jolla Institute for Allergy and Immunology, La Jolla, CA) and C.A. Lowell (University of California, San Francisco [UCSF], San Francisco, CA), respectively. *S1pr1*$^{f/f}$ (Allende et al., 2003), *Cd19*$^{-/-}$ (MGI; 88319), *Cxcr5*$^{-/-}$ (MGI; 103567; Förster et al., 1994), HEL-specific MD4 Ig transgenic (MGI; 2384162), soluble HEL ML5 transgenic (MGI; 2384160), $OVA_{323–339}$-specific TCR transgenic OT-II (MGI; 3046083), *Cd169*$^{DTR/+}$ (MGI; 3720841; Asano et al., 2011, *Itgb1*$^{fl/fl}$ (MGI; 192649), and *Itgb2*$^{-/-}$ (MGI; 1857208) mice were from an internal colony. All mice were maintained under specific pathogen–free conditions in the Laboratory Animal Research Center at UCSF, and all animal procedures were approved by the UCSF Institutional Animal Use and Care Committee. For BM chimeras, mice were lethally irradiated with 550 rad γ-irradiation in two doses 3 h apart and transferred i.v. with BM cells from donors of indicated genotypes. Chimeras were analyzed 6–10 wk after reconstitution. FTY720 treatment was with 30 µg of FTY720 in 200 µl of saline, or saline alone, injected i.v. In vivo pulse labeling was with 1 µg of PE-conjugated anti-CD45.2 or anti-CD11c injected i.v., and mice were analyzed after 3 min. For integrin blockade, mice were treated with 100 µg of anti-α4 (PS/2; Bio X Cell) and 100 µg of anti-αL (M17/4; Bio X Cell) injected i.v., and mice were analyzed after 15 h.

Adoptive transfer and immunizations

For analysis of OTII T cell response, 2×10^5 naive CellTrace violet–labeled OTII T cells were i.v. injected into mice and immunized with OVA-conjugated SRBCs or soluble 20 µg OVA plus 1 µg LPS. Procedures for conjugating OVA to SRBCs have been described previously (Getahun and Heyman, 2009; Yi and Cyster, 2013). 1 ml SRBCs were resuspended in 1 ml PBS containing 30 mg/ml OVA (Sigma-Aldrich) with 250 µl of 100 mg/ml 1-ethyl-3-(3-dimethylaminopropyl)carbodiimide (Sigma-Aldrich) in PBS and incubated for 1 h on ice. Afterward, the SRBCs were washed three times in PBS. For SRBC conjugation with PKH26, 1 ml SRBCs were resuspended with 1 ml conjugation buffer with 4 µl PKH26 dye according to the manual instruction for 20 min, then were washed three times with PBS. 80 µl PKH26-labeled SRBCs were injected i.v. into each mouse, 3 h before analysis. For all experiments between neonates and adults, all injections were done retroorbitally. For MZ B cell reconstitution, 10^7 purified B cells from *Cxcr5*$^{-/-}$ mice were transferred into CD19 KO mice for 2 mo before saline or FTY720 treatment.

Immunofluorescent staining

Cryosections of 10 µm were fixed by acetone for 10 min, dried for 1 h, and stained with goat anti-IgD, FITC-conjugated anti-Marco (Bio-Rad), FITC-conjugated anti-CD169 (BioLegend), biotin-conjugated 33D1 (BioLegend), streptavidin-AF647 (Thermo Fisher Scientific), and AMCA-conjugated donkey anti-goat IgG (H+L; Jackson Immunoresearch). Primary antibody incubation

was performed overnight at 4°C, followed by secondary staining for 3 h at room temperature. For staining of 33D1 (anti-DCIR2), the tyramide amplification kit was used (TSA Biotin System) according to the manual. Images were captured with a Zeiss AxioOberver Z1 inverted microscope and stitched by Zen software.

Macrophage depletion

For clodronate liposome treatment (standard macrophage depletion kit; Encapsula NanoSciences), 100 µg clodronate liposomes or control (Encapsomes) were injected i.v. into mice, and analysis was performed 2–3 wk after treatment. Using *Cd169*$^{DTR/+}$ transgenic mice, 0.75 µg diphtheria toxin (EMD Biosciences) was injected i.p., and analysis was performed 2–3 d after treatment.

Flow cytometry

Single-cell suspensions of splenic cells were washed, blocked with 2.4G2 antibody (Bio X cell), and stained with antibodies of indicated specificities in MACS buffer (PBS and 1% FBS). Staining reagents included BV786 anti-B220 (RA3-6B2), eFluor450 anti-CD8a (53-6.7), FITC anti-CD21 (7E9), APC anti-CD23 (B3B4), PerCP/Cy5.5 anti-MHCII (M5/114.15.2), BV605 anti-CXCR5 (L138D7), APC anti-33D1 (33D1), PE/Cy7 anti-CD279 (RMP1-30), PE anti-CD45.2 (104), biotinylated anti-DCIR2 (33D1), biotinylated anti-CD29 (Itgb1; HMβ1-1) and BV605 anti-CD86 (GL-1) from BioLegend; biotinylated anti-CD18 (Itgb2; C71/16), streptavidin-BV711, and streptavidin-BV605 from BD Biosciences; PE/Cy7 anti-CD11c (N418) from Tonbo Bio; FITC anti-CD49d (Itgα4; R1-2) from Miltenyi Biotec; unconjugated anti-CD11a (Itgal; 121/7) from Southern Biotech; and Cy5 donkey anti-rat IgG and FITC donkey anti-rat IgG from Jackson Immunoresearch. Dead cell exclusion was based on Fixable Viability Dye eFluor 780 staining (eBioscience), and non-singlet events were excluded with forward scatter width/height characteristics. All data were collected on an LSR II cytometer (BD) and analyzed with FlowJo software (TreeStar).

Quantitative PCR

Follicular B cells (B220^{+} CD21^{int} CD23^{+}) and MZ B cells (B220^{+} CD21^{hi} CD23^{lo}) from mice of the indicated genotypes were sorted with a FACS Aria III. cDC2 (MHCII^{hi} CD11c^{hi} 33D1^{+}) and cDC1 (MHCII^{hi} CD11c^{hi} CD8^{+}) were enriched by CD11c MicroBeads from Miltenyi Biotec, and then sorted. Total RNA samples were extracted with the Direct-zol RNA Microprep kit (Zymo Research) and reverse-transcribed with RevertAid First Strand cDNA Synthesis Kit. A StepOnePlus real-time PCR system (Applied Biosystems) with iTaq SYBR Green Supermix (Bio-Rad) and the appropriate primer pairs (Integrated DNA Technologies) were used for real-time PCR. The following primers were used: *S1pr1* forward, 5′-GTGTAGACCCAGAGTCCTGCG-3′; reverse, 5′-AGCTTTTCCTTGGCTGGAGAG-3′; and *Gapdh* forward, 5′-TGTTCCTACCCCCAATGTGTC-3′; reverse, 5′-TAGCCCAAGATGCCCTTCAGT-3′.

S1pr1$^{\Delta Ex2}$ allele detection

cDC2 cells (MHCII^{hi} CD11c^{hi} DCIR2^{+}) and cDC1 cells (MHCII^{hi} CD11c^{hi} CD8^{+}) were enriched by CD11c MicroBeads from Miltenyi Biotec, and then sorted with a FACS Aria III. DNA was extracted by QuickExtract DNA Extraction Solution (Epicentre). *S1pr1*$^{\Delta Ex2}$ allele was detected by PCR. The following primers were used: P1, 5′-GAGCGGAGGAAGTTAAAAGTG-3′, and P2, 5′-GATCCTAAGGCAATGTCCTAGAATGGGACA-3′.

Statistical analysis

Statistics and graphing were done with Prism (GraphPad). Except when noted otherwise, two-tailed Student's *t* tests were used to compare endpoint means of different groups.

Online supplemental material

Fig. S1 shows the representative distribution patterns of in vivo pulse-labeled DCIR2^{+} cDC2s in the neonatal and adult spleen. Fig. S2 shows the cDC2 location in follicles in CXCR5-deficient mice and that *Cxcr5*$^{-/-}$ MZ B cell reconstitution in *Cd19*$^{-/-}$ mice blocks FTY720-induced cDC2 relocalization. Fig. S3 shows the role for integrins in supporting the maintenance of cDC2s in blood-exposed regions of the spleen.

Acknowledgments

We thank Reinhold Forster (Medizinische Hochschule, Hannover, Germany), Klaus Ley (La Jolla Institute for Immunology, San Diego, CA), and Masato Tanaka (Tokyo University of Pharmacy and Life Sciences, Tokyo, Japan) for mice and Li-Shu Wang (Medical College of Wisconsin, Milwaukee, WI) and Jianhua Yu (City of Hope National Medical Center, Duarte, CA) for *Gpr43*$^{-/-}$ BM.

D. Liu was supported by a Cancer Research Institute Irvington Fellowship, J. Wu was the recipient of a postdoctoral fellowship from the Damon Runyon Cancer Research Foundation, and J.G. Cyster is a Howard Hughes Medical Institute investigator. This work was supported in part by National Institutes of Health grant AI40098.

Author contributions: D. Liu and J.G. Cyster conceived the project; D. Liu designed and conducted the experiments; J. Wu made initial observations in integrin-deficient mice; J. An genotyped mice; and D. Liu and J.G. Cyster analyzed the data and wrote the manuscript.

Disclosures: J. Cyster reported consulting for several biotech companies and serving on the scientific advisory board of ALX Oncology Inc. and MiroBio Ltd. No other disclosures were reported.

Submitted: 6 December 2019
Revised: 6 May 2020
Accepted: 24 June 2020

References

Allende, M.L., T. Yamashita, and R.L. Proia. 2003. G-protein-coupled receptor S1P1 acts within endothelial cells to regulate vascular maturation. *Blood*. 102:3665–3667. https://doi.org/10.1182/blood-2003-02-0460

Ansel, K.M., V.N. Ngo, P.L. Hyman, S.A. Luther, R. Förster, J.D. Sedgwick, J.L. Browning, M. Lipp, and J.G. Cyster. 2000. A chemokine-driven positive feedback loop organizes lymphoid follicles. *Nature*. 406:309–314. https://doi.org/10.1038/35018581

Arnon, T.I., R.M. Horton, I.L. Grigorova, and J.G. Cyster. 2013. Visualization of splenic marginal zone B-cell shuttling and follicular B-cell egress. *Nature*. 493:684–688. https://doi.org/10.1038/nature11738

Asano, K., A. Nabeyama, Y. Miyake, C.H. Qiu, A. Kurita, M. Tomura, O. Kanagawa, S. Fujii, and M. Tanaka. 2011. CD169-positive macrophages dominate antitumor immunity by crosspresenting dead cell-associated antigens. *Immunity*. 34:85–95. https://doi.org/10.1016/j.immuni.2010.12.011

Balázs, M., F. Martin, T. Zhou, and J. Kearney. 2002. Blood dendritic cells interact with splenic marginal zone B cells to initiate T-independent immune responses. *Immunity*. 17:341–352. https://doi.org/10.1016/S1074-7613(02)00389-8

Briseño, C.G., A.T. Satpathy, J.T. Davidson, IV, S.T. Ferris, V. Durai, P. Bagadia, K.W. O'Connor, D.J. Theisen, T.L. Murphy, and K.M. Murphy. 2018. Notch2-dependent DC2s mediate splenic germinal center responses. *Proc. Natl. Acad. Sci. USA*. 115:10726–10731. https://doi.org/10.1073/pnas.1809925115

Cahalan, S.M., P.J. Gonzalez-Cabrera, G. Sarkisyan, N. Nguyen, M.T. Schaeffer, L. Huang, A. Yeager, B. Clemons, F. Scott, and H. Rosen. 2011. Actions of a picomolar short-acting $S1P_1$ agonist in $S1P_1$-eGFP knock-in mice. *Nat. Chem. Biol.* 7:254–256. https://doi.org/10.1038/nchembio.547

Calabro, S., D. Liu, A. Gallman, M.S. Nascimento, Z. Yu, T.T. Zhang, P. Chen, B. Zhang, L. Xu, U. Gowthaman, et al. 2016. Differential Intrasplenic Migration of Dendritic Cell Subsets Tailors Adaptive Immunity. *Cell Rep.* 16:2472–2485. https://doi.org/10.1016/j.celrep.2016.07.076

Calderwood, D.A., I.D. Campbell, and D.R. Critchley. 2013. Talins and kindlins: partners in integrin-mediated adhesion. *Nat. Rev. Mol. Cell Biol.* 14:503–517. https://doi.org/10.1038/nrm3624

Caton, M.L., M.R. Smith-Raska, and B. Reizis. 2007. Notch-RBP-J signaling controls the homeostasis of CD8- dendritic cells in the spleen. *J. Exp. Med.* 204:1653–1664. https://doi.org/10.1084/jem.20062648

Cinamon, G., M. Matloubian, M.J. Lesneski, Y. Xu, C. Low, T. Lu, R.L. Proia, and J.G. Cyster. 2004. Sphingosine 1-phosphate receptor 1 promotes B cell localization in the splenic marginal zone. *Nat. Immunol.* 5:713–720. https://doi.org/10.1038/ni1083

Cinamon, G., M.A. Zachariah, O.M. Lam, F.W. Foss, Jr., and J.G. Cyster. 2008. Follicular shuttling of marginal zone B cells facilitates antigen transport. *Nat. Immunol.* 9:54–62. https://doi.org/10.1038/ni1542

Czeloth, N., A. Schippers, N. Wagner, W. Müller, B. Küster, G. Bernhardt, and R. Förster. 2007. Sphingosine-1 phosphate signaling regulates positioning of dendritic cells within the spleen. *J. Immunol.* 179:5855–5863. https://doi.org/10.4049/jimmunol.179.9.5855

Dominguez, G.A., N.R. Anderson, and D.A. Hammer. 2015. The direction of migration of T-lymphocytes under flow depends upon which adhesion receptors are engaged. *Integr. Biol.* 7:345–355. https://doi.org/10.1039/C4IB00201F

Dudziak, D., A.O. Kamphorst, G.F. Heidkamp, V.R. Buchholz, C. Trumpfheller, S. Yamazaki, C. Cheong, K. Liu, H.W. Lee, C.G. Park, et al. 2007. Differential antigen processing by dendritic cell subsets in vivo. *Science*. 315:107–111. https://doi.org/10.1126/science.1136080

Durai, V., and K.M. Murphy. 2016. Functions of Murine Dendritic Cells. *Immunity*. 45:719–736. https://doi.org/10.1016/j.immuni.2016.10.010

Eisenbarth, S.C.. 2019. Dendritic cell subsets in T cell programming: location dictates function. *Nat. Rev. Immunol.* 19:89–103. https://doi.org/10.1038/s41577-018-0088-1

Fasnacht, N., H.Y. Huang, U. Koch, S. Favre, F. Auderset, Q. Chai, L. Onder, S. Kallert, D.D. Pinschewer, H.R. MacDonald, et al. 2014. Specific fibroblastic niches in secondary lymphoid organs orchestrate distinct Notch-regulated immune responses. *J. Exp. Med.* 211:2265–2279. https://doi.org/10.1084/jem.20132528

Förster, R., T. Emrich, E. Kremmer, and M. Lipp. 1994. Expression of the G-protein--coupled receptor BLR1 defines mature, recirculating B cells and a subset of T-helper memory cells. *Blood*. 84:830–840. https://doi.org/10.1182/blood.V84.3.830.bloodjournal843830

Forsthuber, T., H.C. Yip, and P.V. Lehmann. 1996. Induction of TH1 and TH2 immunity in neonatal mice. *Science*. 271:1728–1730. https://doi.org/10.1126/science.271.5256.1728

Gatto, D., K. Wood, I. Caminschi, D. Murphy-Durland, P. Schofield, D. Christ, G. Karupiah, and R. Brink. 2013. The chemotactic receptor EBI2 regulates the homeostasis, localization and immunological function of splenic dendritic cells. *Nat. Immunol.* 14:446–453. https://doi.org/10.1038/ni.2555

Getahun, A., and B. Heyman. 2009. Studies on the mechanism by which antigen-specific IgG suppresses primary antibody responses: evidence for epitope masking and decreased localization of antigen in the spleen. *Scand. J. Immunol.* 70:277–287. https://doi.org/10.1111/j.1365-3083.2009.02298.x

Lewis, K.L., M.L. Caton, M. Bogunovic, M. Greter, L.T. Grajkowska, D. Ng, A. Klinakis, I.F. Charo, S. Jung, J.L. Gommerman, et al. 2011. Notch2 receptor signaling controls functional differentiation of dendritic cells in the spleen and intestine. *Immunity*. 35:780–791. https://doi.org/10.1016/j.immuni.2011.08.013

Li, J., E. Lu, T. Yi, and J.G. Cyster. 2016. EBI2 augments Tfh cell fate by promoting interaction with IL-2-quenching dendritic cells. *Nature*. 533:110–114. https://doi.org/10.1038/nature17947

Loder, F., B. Mutschler, R.J. Ray, C.J. Paige, P. Sideras, R. Torres, M.C. Lamers, and R. Carsetti. 1999. B cell development in the spleen takes place in discrete steps and is determined by the quality of B cell receptor-derived signals. *J. Exp. Med.* 190:75–89. https://doi.org/10.1084/jem.190.1.75

Lu, T.T., and J.G. Cyster. 2002. Integrin-mediated long-term B cell retention in the splenic marginal zone. *Science*. 297:409–412. https://doi.org/10.1126/science.1071632

Lu, E., E.V. Dang, and J.G. Cyster. 2017. Distinct oxysterol requirements for positioning naive and activated dendritic cells in the spleen. *Sci. Immunol.* 2:eaal5237.

Martin, F., and J.F. Kearney. 2002. Marginal-zone B cells. *Nat. Rev. Immunol.* 2:323–335. https://doi.org/10.1038/nri799

Mason, D.Y., M. Jones, and C.C. Goodnow. 1992. Development and follicular localization of tolerant B lymphocytes in lysozyme/anti-lysozyme IgM/IgD transgenic mice. *Int. Immunol.* 4:163–175. https://doi.org/10.1093/intimm/4.2.163

Mebius, R.E., and G. Kraal. 2005. Structure and function of the spleen. *Nat. Rev. Immunol.* 5:606–616. https://doi.org/10.1038/nri1669

Miyake, Y., K. Asano, H. Kaise, M. Uemura, M. Nakayama, and M. Tanaka. 2007. Critical role of macrophages in the marginal zone in the suppression of immune responses to apoptotic cell-associated antigens. *J. Clin. Invest.* 117:2268–2278. https://doi.org/10.1172/JCI31990

Petrich, B.G., P. Marchese, Z.M. Ruggeri, S. Spiess, R.A. Weichert, F. Ye, R. Tiedt, R.C. Skoda, S.J. Monkley, D.R. Critchley, et al. 2007. Talin is required for integrin-mediated platelet function in hemostasis and thrombosis. *J. Exp. Med.* 204:3103–3111. https://doi.org/10.1084/jem.20071800

Ridge, J.P., F. Di Rosa, and P. Matzinger. 1998. A conditioned dendritic cell can be a temporal bridge between a CD4+ T-helper and a T-killer cell. *Nature*. 393:474–478. https://doi.org/10.1038/30989

Sarzotti, M., D.S. Robbins, and P.M. Hoffman. 1996. Induction of protective CTL responses in newborn mice by a murine retrovirus. *Science*. 271:1726–1728. https://doi.org/10.1126/science.271.5256.1726

Satpathy, A.T., C.G. Briseño, J.S. Lee, D. Ng, N.A. Manieri, W. Kc, X. Wu, S.R. Thomas, W.L. Lee, M. Turkoz, et al. 2013. Notch2-dependent classical dendritic cells orchestrate intestinal immunity to attaching-and-effacing bacterial pathogens. *Nat. Immunol.* 14:937–948. https://doi.org/10.1038/ni.2679

Tedford, K., M. Steiner, S. Koshutin, K. Richter, L. Tech, Y. Eggers, I. Jansing, K. Schilling, A.E. Hauser, M. Korthals, et al. 2017. The opposing forces of shear flow and sphingosine-1-phosphate control marginal zone B cell shuttling. *Nat. Commun.* 8:2261. https://doi.org/10.1038/s41467-017-02482-4

Wu, J., H. Wu, J. An, C.M. Ballantyne, and J.G. Cyster. 2018. Critical role of integrin CD11c in splenic dendritic cell capture of missing-self CD47 cells to induce adaptive immunity. *Proc. Natl. Acad. Sci. USA*. 115:6786–6791. https://doi.org/10.1073/pnas.1805542115

Yi, T., and J.G. Cyster. 2013. EBI2-mediated bridging channel positioning supports splenic dendritic cell homeostasis and particulate antigen capture. *eLife*. 2. e00757. https://doi.org/10.7554/eLife.00757

Yi, T., J. Li, H. Chen, J. Wu, J. An, Y. Xu, Y. Hu, C.A. Lowell, and J.G. Cyster. 2015. Splenic Dendritic Cells Survey Red Blood Cells for Missing Self-CD47 to Trigger Adaptive Immune Responses. *Immunity*. 43:764–775. https://doi.org/10.1016/j.immuni.2015.08.021

You, Y., H. Zhao, Y. Wang, and R.H. Carter. 2009. Cutting edge: Primary and secondary effects of CD19 deficiency on cells of the marginal zone. *J. Immunol.* 182:7343–7347. https://doi.org/10.4049/jimmunol.0804295

Supplemental material

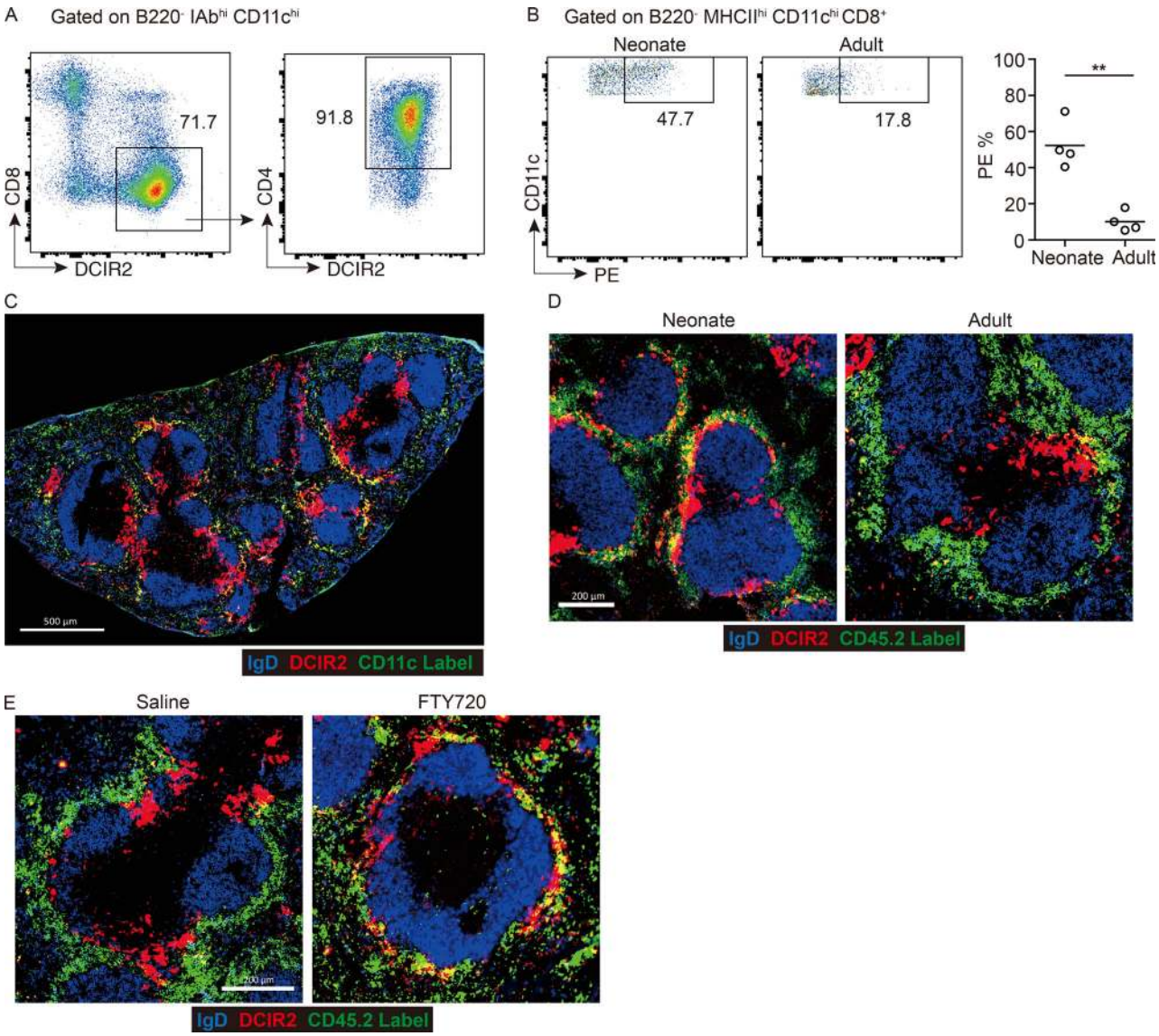

Figure S1. **Representative distribution patterns of in vivo pulse-labeled DCIR2⁺ cDC2s. (A)** Representative FACS profiles displaying gate between CD4 and DCIR2 in DCIR2⁺ CD8⁻ cDC2 cells. **(B)** FACS profiles and frequencies of in vivo anti-CD45-PE–labeled CD8⁺ cDC1s in mice of the indicated ages. Each symbol represents one mouse, and lines denote means. One of three independent experiments with similar results is shown, in which each group had at least three mice. **(C)** In vivo antibody labeling of DCIR2⁺ cDC2s (red) relative to IgD⁺ B cells (blue) in spleens 3 min after i.v. injection of PE-conjugated anti-CD11c (green). Blood-exposed DCIR2⁺ DCs (cells that have bound CD11c-PE) appear yellow. Multiple images are stitched to obtain the full spleen view. Scale bar, 500 µm. **(D and E)** Representative views of spleens 3 min after i.v. injection of PE-conjugated anti-CD45 (green) from the mice of the indicated ages (D) or spleens of adult mice 4 h after saline or FTY720 treatment (E). Blood-exposed DCIR2⁺ DCs (cells that have bound CD45.2-PE) appear yellow. Scale bar, 200 µm. Sections are representative of multiple cross sections from five mice of each type. **, P < 0.01.

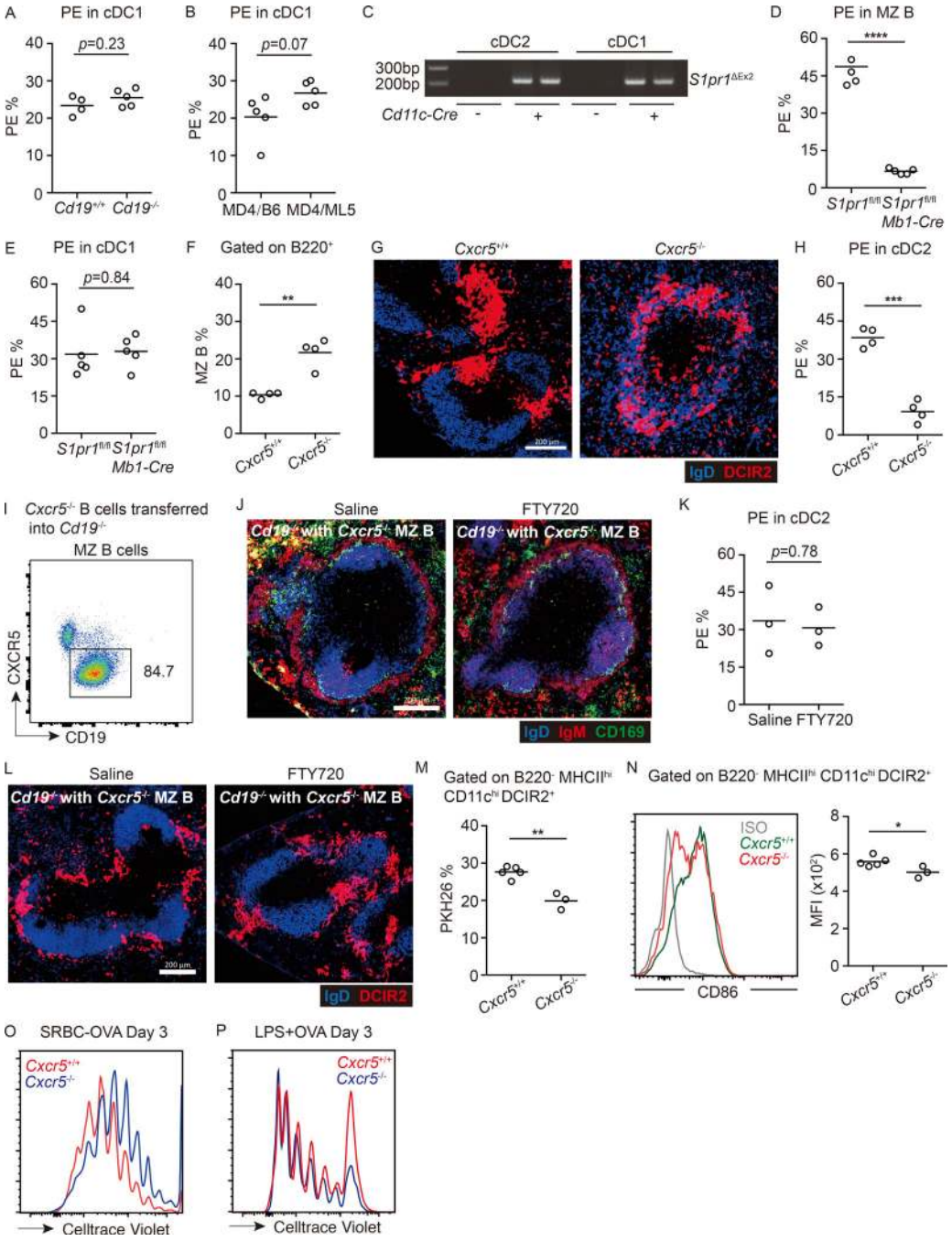

Figure S2. **Most cDC2s are located in follicles in CXCR5-deficient mice, whereas *Cxcr5*$^{-/-}$ MZ B cells in *Cd19*$^{-/-}$ mice block FTY720-induced cDC2 relocalization. (A)** Frequencies of in vivo anti-CD45-PE–labeled CD8^{+} cDC1s in *Cd19*$^{+/+}$ and *Cd19*$^{-/-}$ chimeras. **(B)** Frequencies of in vivo anti-CD45-PE–labeled CD8^{+} cDC1s in MD4/B6 and MD4/ML5 chimeras. Each symbol represents one mouse, and lines denote means. Data are pooled from two independent experiments. **(C)** Gel image of Cd11c-Cre–mediated recombination of *S1pr1*^{loxP} using cDC2 and cDC1 DNA samples. *S1pr1*$^{\Delta Ex2}$, *S1pr1* allele after Cre-mediated recombination. **(D and E)** Frequencies of in vivo anti-CD45-PE–labeled MZ B cells (D) and cDC1s (E) in spleens of indicated genotyped BM chimeras. Each symbol represents one mouse, and lines denote means. Data are pooled from two independent experiments. **(F–H)** Frequencies of CD21^{hi} CD23^{lo} MZ B cells in total B220^{+} B cells (F), of in vivo anti-CD45-PE–labeled cDC2s (H), and representative distribution patterns of DCIR2^{+} cDC2s (red) relative to IgD^{+} B cells (blue) in spleens (G) of mice of the indicated types. Scale bar, 200 µm. **(I–L)** *Cxcr5*$^{-/-}$ MZ B cells in *Cd19*$^{-/-}$ mice restrict cDC2 access. **(I)** Representative profile of *Cxcr5*$^{-/-}$ MZ B cell reconstitution 2 mo after transfer. **(J)** Representative distribution patterns of IgM^{hi} MZ B cells (red) and CD169^{+} MMMs relative to IgD^{+} follicular B cells (blue) in spleens of 4-h saline- or FTY720-treated mice. Scale bar, 200 µm. **(K and L)** Frequencies of in vivo anti-CD45-PE–labeled cDC2s (K) and representative distribution patterns of DCIR2^{+} cDC2s (red) relative to IgD^{+} B cells (blue) in spleens (L) of 4-h saline- or FTY720-treated mice. Scale bar, 200 µm. **(M)** Frequencies of PKH26-dye acquisition in DCIR2^{+} cDC2s of indicated genotypes 3 h after immunization with PKH26-labeled SRBCs. **(N)** Mean fluorescence intensity (MFI) and representative histogram of surface CD86 expression on cDC2s from mice treated as in M. **(O and P)** Representative FACS plot of proliferation of transferred OT-II T cells in mice of the indicated genotype at day 3 after SRBCs-OVA (O) or OVA plus LPS (P) immunization. Each symbol represents one mouse, and lines denote means. One of two independent experiments with similar results is shown, in which each group had at least three mice. Sections are representative of multiple spleen cross sections from five mice of each type. *, P < 0.05; **, P < 0.01; ***, P < 0.001; ****, P < 0.0001.

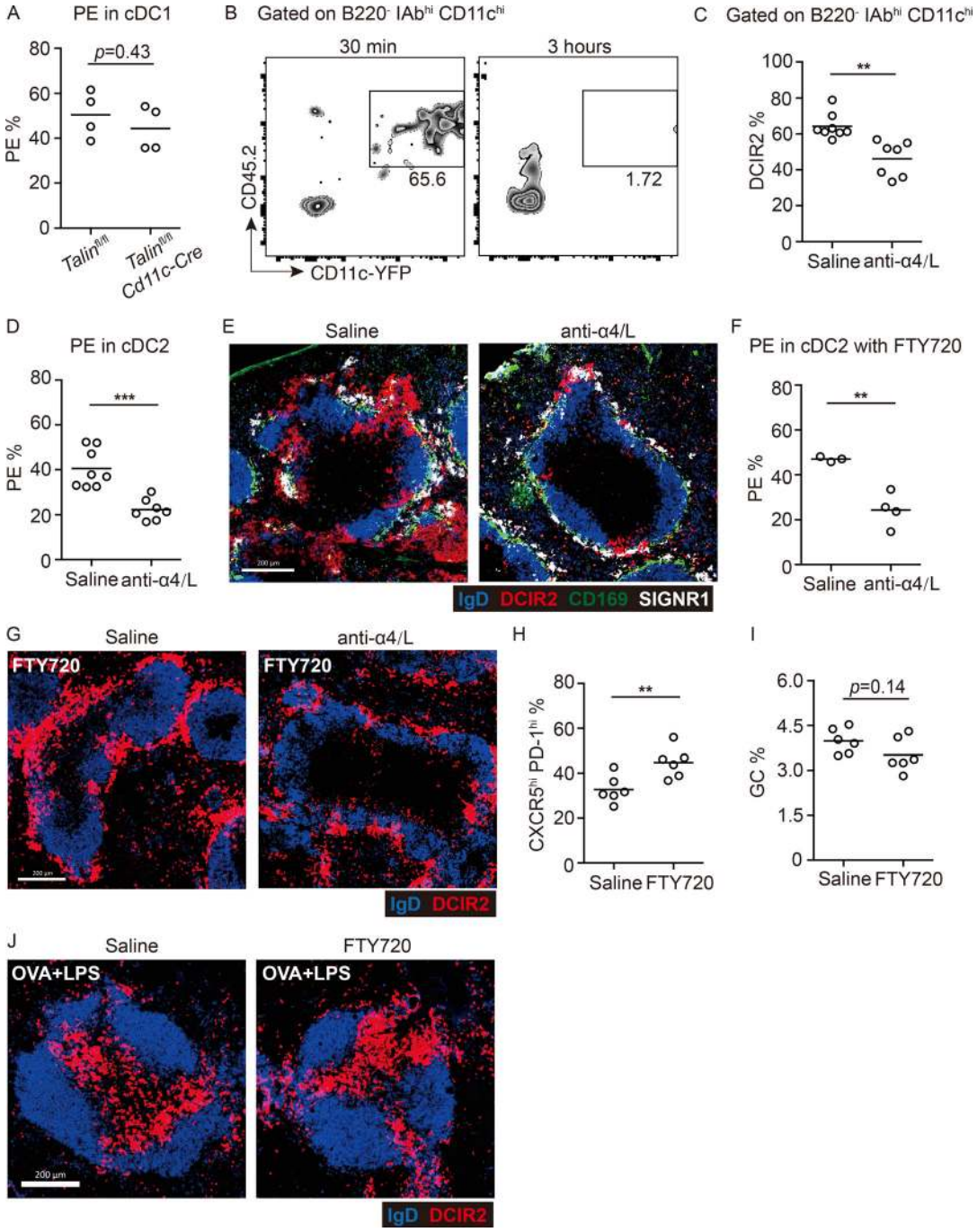

Figure S3. **Integrins are required for the maintenance of cDC2s in blood-exposed regions of spleen. (A)** Frequencies of in vivo anti-CD45-PE–labeled $CD8^+$ cDC1s in *Cd11c-Cre Talin*$^{fl/fl}$ and control mice. Each symbol represents one mouse, and lines denote means. One of two independent experiments with similar results is shown. **(B)** Total splenocytes isolated from Cd11c-YFP reporter mice ($CD45.2^+$) were transferred into $CD45.1^+$ mice. Representative profiles of transferred DCs in blood after 30 min and 3 h. One of two independent experiments with similar results is shown, in which each group had at least three mice. **(C–E)** Frequencies of $DCIR2^+$ cDC2s in spleen (C) and of in vivo anti-CD45-PE labeling of cDC2s (D) or representative distribution patterns of $DCIR2^+$ cDC2s (red), $CD169^+$ MMMs (green), and $SIGNR1^+$ MZMs (white) relative to IgD^+ B cells (blue) in spleens 15 h after anti-α4/αL or saline treatment (E). Each symbol represents one mouse, and lines denote means. Data are pooled from two independent experiments. Scale bar, 200 µm. **(F and G)** Frequencies of in vivo anti-CD45-PE labeling of cDC2s (F) or representative distribution patterns of $DCIR2^+$ cDC2s (red) relative to IgD^+ B cells (blue) in spleens 4 h after FTY720 and 15 h after anti-α4/αL or saline treatment (G). Scale bar, 200 µm. **(H and I)** Frequencies of $CXCR5^{hi}$ $PD\text{-}1^{hi}$ T cells among transferred OT-II T cells (H) or FAS^{hi} $GL7^{hi}$ GC B cells in $B220^+$ B cells (I) in 4-h FTY720- or saline-pretreated mice, 6 d after SRBC-OVA immunization. **(J)** Representative distribution patterns of $DCIR2^+$ cDC2s (red) relative to IgD^+ B cells (blue) in spleens 5 h after soluble OVA plus LPS immunization. Scale bar, 200 µm. Each symbol represents one mouse, and lines denote means. One of two independent experiments with similar results is shown. Sections are representative of multiple spleen cross sections from six mice of each type. **, $P < 0.01$; ***, $P < 0.001$.